Microseismic Imaging of Hydrofractures with the Aid of Conical Waves

DP1.2

David C. Ilderton, Tadeusz W. Patzek, James W. Rector, University of California, Berkeley; and Harold J. Vinegar, Shell Development Co.*

SUMMARY

Optimal production of oil from the South Belridge oil field depends on the accurate characterization of hydraulic fractures. This paper presents an extension of the passive imaging work done by Vinegar *et al.*, (1991). A hydrofracture induced in the South Belridge reservoir was imaged using seismic data acquired from three dedicated observation wells. These wells recorded microseismic events produced during the hydrofracturing process. We had to invert for the event locations using only shear wave arrivals because no compressional wave arrivals were detected.

Our initial inversion assuming a homogeneous velocity model yielded unsatisfactory results. The microseismic event locations failed to reveal a clearly defined fracture plane. However, the excitation of tube waves in the treatment well by nearby microseismic events led to the detection of conical waves by the geophones. These conical wave arrivals provided a means by which to estimate a 'relative' velocity field.

Choosing a reference velocity and a reference direction toward one observation well, we were able to calculate relative velocities toward the other observations wells and establish a heterogeneous velocity model. Inverting for the locations of the microseismic events with this new model resulted in a much more defined fracture plane. We now hope to develop a time variable heterogeneous velocity model since the conical wave arrivals occur fairly regularly throughout our data.

INTRODUCTION

The hydrofracturing of reservoirs is an important method for enhancing oil production. For the South Belridge diatomite oil field located near Bakersfield, California, the technique is indisputably essential due to the rock's extremely low permeability. To optimize the array of producing wells in the field, the parameters of the hydrofractures must be accurately determined. These parameters, including height, length, azimuth, and symmetry, are used to space and orient producing and injecting wells.

Vinegar *et al.*, (1991) showed that the geometry of hydrofractures could be imaged actively, using shear wave shadowing, and passively, using microseismic events produced as the rock is cracked and propped open. In the case of passive imaging, the microseismic event arrival times are picked and inverted to find the event locations, which are then used to infer the hydrofracture geometry as a function of time. As in any arrival time based inversion, the inferred event locations are very sensitive to the chosen formation velocity. It is therefore necessary to determine a background (potentially time variable) velocity field to accurately invert for the event locations.

In this study we extend the analysis of Vinegar *et al.*, (1991) on passive imaging of a hydrofracture in the South Belridge oil field by incorporating a space and time variable velocity function into the inversion of microseismic events. We use conical waves emitted by tube waves excited in the treatment well to calculate the azimuthal variation in the formation shear velocity. A velocity (pre-determined from perforation shots) is assigned to a preferred direction, and the velocities in other directions are calculated from the conical wave arrival times. Using this spatially variable subsurface velocity model, the microseismic event locations collapse down to a well defined plane. Since the conical waves are produced during the entire fracturing process, we can estimate a time variable velocity field.

DATA ACQUISITION

Figure 1 shows a plan view of the South Belridge field site taken from Vinegar *et al.*, (1991). The treatment well A (the study by Vinegar *et al.* was done for treatment well C) is surrounded by three dedicated remote geophone wells MO1 (Microseismic Observation 1), MO2, and MO3. For MO2 and MO3, the vertical component of thirteen geophones was recorded throughout the entire hydrofracturing process while twelve geophones were recorded in MO1. The depth interval of the geophones was about 1000 to 1550 feet (300 to 475 meters) in each of the three wells. The hydrofracture lasted about five hours and consisted of four mini fracture stages followed by a main fracture stage.

As the rock fractured, microseismic events were produced and detected by the geophones as shear wave direct arrivals. No compressional wave arrivals were detected, but about 50 shear wave arrivals were recorded, 20 percent of which were conical waves. The conical waves appear to be produced by microseismic events located near the treatment well. When present, the conical waves obscured the S-wave direct arrivals, making it impossible to estimate microseismic event locations from these arrivals.

We believe that the absence of P-waves is either due to the very large porosity of the diatomite, making it incapable of supporting P-waves, or due to the radiation pattern of the microseismic event focal mechanism, (Aki and Richards, 1980). It is this lack of P-wave arrivals which makes our situation unique in that we cannot use traveltime differences between P-wave and S-wave arrivals to locate our events as is done in earthquake seismology.

INITIAL MICROSEISMIC EVENT LOCATIONS

Since we only recorded shear wave arrivals in this experiment, we had to use the moveout of the S-wave arrivals to find the source locations of the microseismic events. The shear velocity in the diatomite was computed as a function of depth from perforation shot data (Vinegar *et al.*, 1991) and found to range from 2000 to 2500 ft/s (610 to 760 m/s). Our initial inversion routine assumed a uniform shear velocity field. After picking the arrival times of the events, we used a "growing circles" algorithm to invert for the locations. The routine employed the Polak-Ribiere conjugate gradient method to find the minimum of a five dimensional tensor. Figure 2 shows the results of the initial inversion. The event locations are more dispersed then we had expected, and it is difficult to define a fracture plane at all. A crumbled zone around the borehole might be a more accurate interpretation. Also, the fracture appears to be asymmetrical, extending four times further toward the northeast than toward the southwest. The results led us to question the validity of a homogeneous shear wave velocity model. The conical waves that had originally been considered as unwanted noise, obscuring the direct arrival energy, were now viewed as a potentially useful tool to estimate the shear wave velocity between the treatment well and the different observation wells.

CONICAL WAVE GENERATION AND PROPAGATION

We believe conical waves are produced by a microseismic event near the treatment well that causes a fluid disturbance which emits tube waves that travel up and down the borehole away from the fracture. This generation mechanism is similar to that observed in VSP data (Cheng and Toksoz, 1984). As the tube wave propagates, it will diffract into the formation as a conical wavefront if the tube wave velocity exceeds the adjacent formation velocity Meredith (1990) and Vinegar *et al.* (1991). In our region, the tube wave velocity is greater than the formation's shear velocity but less than the compressional velocity; hence, we are only involved with shear conical waves. The conical wave propagates in the far field at an angle Θ with respect to the borehole axis perpendicular, where

$$\Theta = \sin^{-1}\left(\frac{V_s(z)}{V_t(z,t)}\right), \qquad (1)$$

$V_s(z)$ is the depth dependent shear velocity of the formation, and V_t is the tube wave velocity. Θ in our case varies from about 28° to 45° and is much more sensitive to V_s than to V_t. Figure 3 shows a diagram illustrating the raypaths taken by the conical waves from Well A to MO1, MO2, and MO3. Note the shadow zone equal to 2Θ separating the conical waves that are created by the upgoing and downgoing tube waves. Consequently, only geophones whose depths are greater or less than the depth of the microseismic event by an amount equal to $r\tan\Theta$, where r is the radial distance from the treatment well, will record strong primary conical wave arrivals.

The tube wave velocity is both depth and *time* dependent (where *time* refers to the time history of the hydrofracture), and its zero frequency approximation is given by Hardage (1992) as :

$$V_t(z,t) = \left[\rho_f(t)\left(\frac{1}{B_f} + \frac{1}{V_s^2(z)\cdot\rho_r + Eh/d}\right)\right]^{-1/2} \qquad (2)$$

where $\rho_f(t)$ is the time dependent well fluid density (It changes with time as different mixtures of proppant and fluid are pumped into the fracture during the hydrofracturing process.), B_f is the bulk modulus of the well fluid, $V_s(z)$ is the depth dependent formation shear velocity, ρ_f is the bulk density of the formation, and E, h, and d are the Young's modulus, wall thickness, and inner diameter of the well casing, respectively. The velocity was computed to be about 4300 ft/s (1310 m/s) and is most sensitive to ρ_f.

Whereas tube waves attenuate exponentially away from the borehole, the conical waves fall off as the square root of the distance from the borehole (White, 1965). Therefore, high energy conical wave arrivals can be recorded at large distances from the treatment well. Figure 4 shows an example of a conical wave arrival in MO2. The linear moveout with receiver depth and apparent velocity of approximately 4300 ft/s (1310 m/s, i.e. the tube wave velocity) characterizes the conical wave in this area.

REPOSITIONING OF MICROSEISMIC EVENTS USING HETEROGENEOUS SHEAR VELOCITY FIELD

Use of Conical Waves to Estimate Shear Velocities

In the calculation of the relative velocities, we assumed straight raypaths for the conical waves from the treatment well to the geophones. We chose as our reference, the direction toward MO2, and the reference shear velocity was computed as a function of depth from perforation shot data (Vinegar *et al.*, 1991) from perforations shot in a nearby well. The emergent angles of the conical wave raypaths from the borehole were calculated using equations (1) and (2). Five raypaths, each at a different depth, were then chosen in such a way as to exactly intersect MO2 at a specific geophone depth while intersecting MO1 and MO3 at depths where a nearby geophone was available.

The modeled traveltime of the conical wave to MO2 was found by dividing the straight ray distance, r_2, from the borehole to MO2 by the reference shear velocity, V_r. The origin time, t_o, of the conical wave 'event' was then calculated by subtracting the modeled traveltime from the picked arrival time, t_{a_2}, at the geophone in MO2

$$t_o = t_{a_2} - \frac{r_2}{V_r}. \qquad (3)$$

The arrival times, $t_{a_{1,3}}$, at the geophones in MO1 and MO3 had to be corrected for the difference in depth, $\Delta z_{1,3}$, between the intersection of the chosen conical wave raypath with these observation wells and the available geophone nearby using

$$t_{c_{1,3}} = t_{a_{1,3}} \pm \frac{\Delta z_{1,3}}{V_t} \qquad (4)$$

where $t_{c_{1,3}}$ is the corrected arrival time in MO1 or MO3, and V_t is the tube wave velocity. This correction assumed parallel raypaths for conical waves emanating at depths that were very close to the depths of the five chosen raypaths. Subtracting the origin time, t_o, from the corrected arrival times at MO1 and MO3 gave the traveltimes of the conical waves to those wells. The relative velocities, $V_{rel_{1,3}}$, were then computed by dividing these traveltimes into the straight ray distances, $r_{1,3}$, to MO1 and MO3

$$V_{rel_{1,3}} = \frac{r_{1,3}}{t_{c_{1,3}} - t_o}. \qquad (5)$$

Figure 5 shows the velocity ratios versus depth for the five chosen raypaths. Note that the velocity towards MO2 (reference direction) is nearly 50 percent greater than that towards MO1 and almost 40 percent greater than the velocity towards MO3. Proof of these velocity ratios can be seen in Figure 6 showing the arrival of a conical wave at each of the fifteen geophones. The receivers have

been sorted by common depth, and the arrivals at the geophones in MO1 and MO3 have been corrected for depth using equation (4) and distance using

$$\Delta t_{1,3} = \frac{r_{1,3} - r_2}{V_r} \quad (6)$$

where $\Delta t_{1,3}$ is the time correction based on the difference in radial distance between MO2 and MO1 or MO3. These arrivals clearly indicate a faster shear velocity towards MO2 than towards MO1 and MO3. The significant difference, up to 40 percent or more, led us to believe that the cause was heterogeneity rather than shear wave birefringence.

Repositioning of Events Using Relative Shear Velocity Field

The real test for our 'relative' shear wave velocity field was to see how its use in the inversion routine affected our initial microseismic event locations. In using the shear velocity field to relocate the events, we assumed that any microseismic arrival recorded at a given observation well propagated to that well with the estimated relative velocity. As shown in Figure 7, the event locations collapsed down to a much more defined fracture plane than those resulting from the use of a uniform velocity field (see Figure 2). Although the hydrofracture length was not significantly changed by the new inversion, the width was decreased by almost 40 percent. This reduction alone was a dramatic improvement and provided justification of our method. The asymmetry of the fracture about the treatment well remained unchanged, but our calculated 'relative' velocities suggest that the fracture may indeed grow asymmetrically. The fact that the shear velocity is much slower towards MO1 than towards MO2 is consistent with our results showing northeast to be the preferred direction of fracturing.

CONCLUSIONS

Imaging the hydrofracture in the South Belridge diatomite with seismic data required a different approach than that used to locate earthquakes because the absence of P-wave arrivals prevented us from using traveltime differences. We were still able to locate the fracture plane using the S-wave events by inverting their arrival times with a "growing circles" algorithm. The use of conical waves to determine a 'relative' velocity field proved to be a significant improvement in calculating the microseismic event locations. Since the same procedure outlined above can be repeated for each stage in the hydrofracturing process, we can develop a *time* dependent 'relative' shear wave velocity field. Inverting each microseismic event with its appropriate velocity field should further enhance our efforts to seismically image hydrofractures.

REFERENCES

Aki, K., Richards, P.G., 1980, Quantitative Seismology: Theory and Methods, W.H. Freeman and Company, San Francisco.

Cheng, C.H., Toksoz, M.N., 1984, Vertical Seismic Profiling, Part B: Advanced Concepts, vol. 14B, Geophysical Press, 276-287.

Hardage, B.A., 1992, Crosswell Seismology and Reverse VSP, vol. 1, Geophysical Press, 147-163.

Meredith, J.A., 1990, Numerical and Analytical Modelling of Downhole Seismic Sources: The Near and Far Field, PhD thesis, Massachusetts Institute of Technology.

Vinegar, H.J., Wills, P.B., DeMartini, D.C., Shlyapobersky, J., Deeg, W.F.J., Adair, R.G., Woerpel, J.C., Fix, J.E., and Sorrells, G.G., 1991, Active and Passive Seismic Imaging of a Hydraulic Fracture in Diatomite, SPE 22756, Proceedings 1991 SPE Annual Technical Conference and Exhibition, Dallas, Texas, Formation Evaluation and Reservoir Geology.

White, J.E., 1965, Seismic Waves: Radiation, Transmission, and Attenuation, McGraw-Hill, Inc., New York.

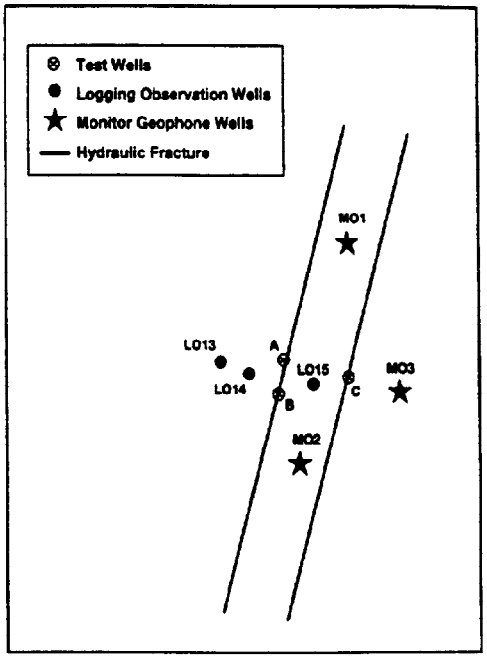

Figure 1: Plan view of test site in the South Belridge field.

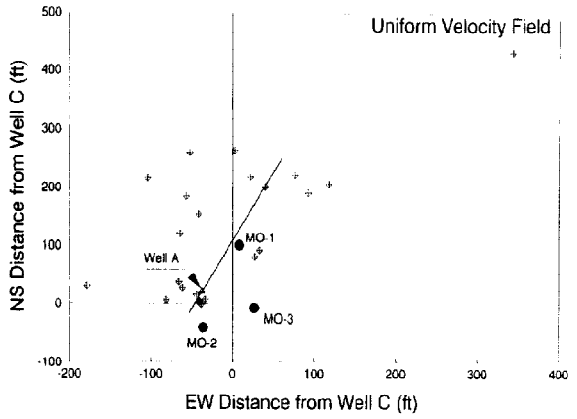

Figure 2: Microseismic event locations using uniform shear velocity model.

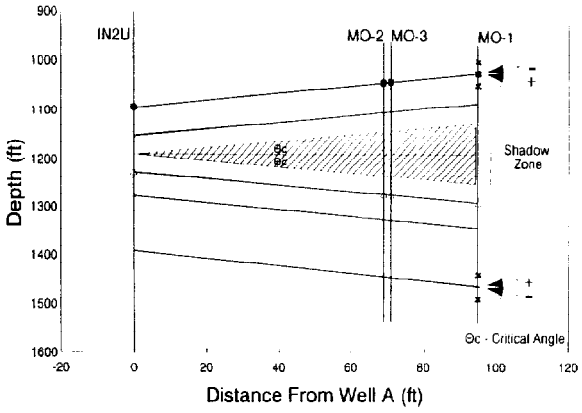

Figure 3: Cross-section showing conical wave raypaths in the test area. Vertical / horizontal scale = 5:1.

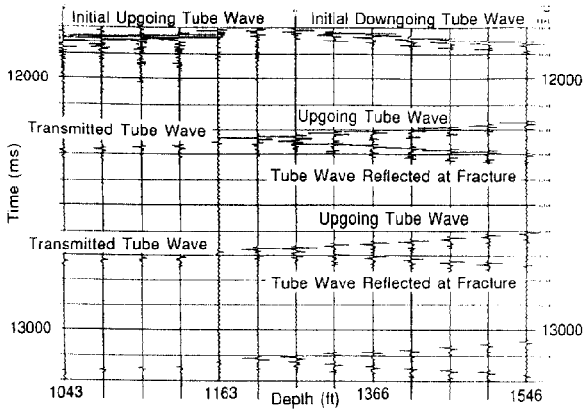

Figure 4: Conical wave arrival as recorded in MO2. Note reverberations due to the tube wave traveling up and down the treatment well and reflecting off the borehole ends.

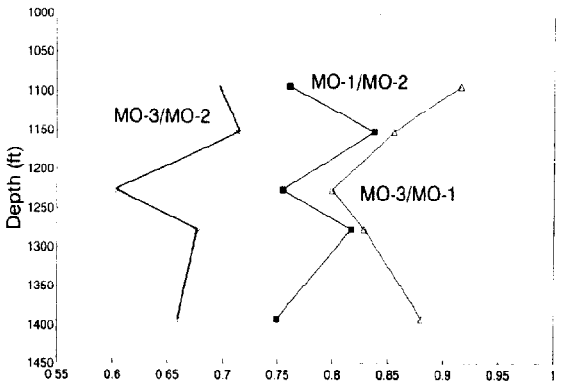

Figure 5: Shear velocity ratios between treatment well and observation wells versus depth using conical wave arrivals.

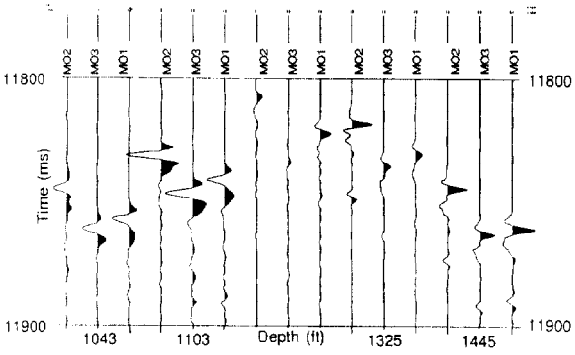

Figure 6: Conical wave arrivals recorded in the fifteen selected geophones. Arrivals in MO1 and MO3 have been time shifted so that raypath lengths are roughly equal. Note the much sooner arrival in MO2 than in MO1 or MO3.

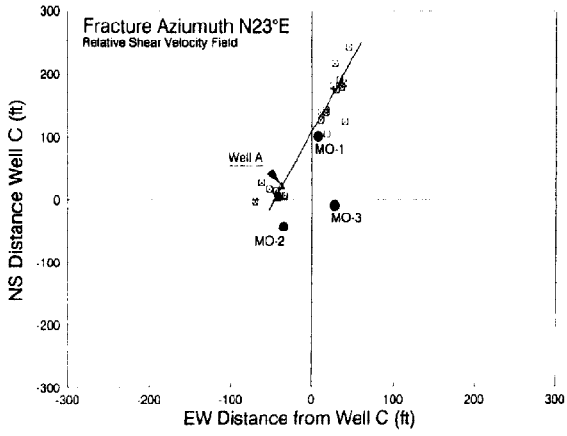

Figure 7: Repositioned microseismic events using heterogeneous shear velocity model.